JOURNAL OF MAGNETIC RESONANCE **127,** 36–48 (1997)
ARTICLE NO. MN971193

Compensation for Spin–Spin Coupling Effects during Adiabatic Pulses

Ēriks Kupče* and Ray Freeman†

*Varian NMR Instruments, 28 Manor Road, Walton-on-Thames, Surrey, KT12 2QF, England; and †Department of Chemistry, University of Cambridge, Lensfield Road, Cambridge CB2 1EW, England

Received February 20, 1997

It is widely recognized that adiabatic fast passage is the most effective method for inverting nuclear spins over a wide range of chemical shifts in situations where radiofrequency power is limited. One possible drawback of an adiabatic sweep is that different groups of spins are inverted at slightly different times, and this can perturb the symmetry of refocusing experiments by appreciable amounts (milliseconds), introducing a serious phase dispersion. We demonstrate how a pair of adiabatic pulses can be used to compensate such refocusing errors. Usually, but not always, this requires the use of two adiabatic pulses with opposite directions of frequency sweep. One important application is the ''isotope filter,'' a scheme for suppressing all proton responses except those from directly bound ^{13}CH groups; a pair of opposed adiabatic pulses allows compensation of refocusing errors over a range of different spin inversion times. In an extension of this technique, a range of ^{13}CH coupling constants can also be accommodated by exploiting the rough linearity between the ^{13}C chemical shift and the magnitude of $^{1}J_{CH}$. Heteronuclear two-dimensional experiments that involve inverting ^{13}C spins during the evolution period can also benefit from a compensating pair of adiabatic pulses, in this case with the same sense of frequency sweep. Finally, a pair of opposed adiabatic pulses is used in a new scheme (''ECHO-WURST'') for suppressing cycling sidebands in broadband heteronuclear decoupling; we show a 500-MHz proton spectrum decoupled from ^{13}C, where the residual cycling sidebands are below 0.06%.

INTRODUCTION

Broadband inversion of nuclear spins can be carried out far more efficiently by adiabatic fast passage (*1*) than by a single hard radiofrequency pulse or by a composite pulse (*2*). This has led to enormous improvements in broadband heteronuclear decoupling techniques (*3–15*), making it possible to cover the entire range of ^{13}C chemical shifts in the highest polarizing fields (18.8 T) of present-day spectrometers, with a radiofrequency intensity as low as $\gamma B_2/2\pi = 3$ kHz. The main penalty for using adiabatic passage appears to be that the sweep duration (a few milliseconds) is considerably longer than that of a comparable composite inversion pulse (a few tens of microseconds). For most high-resolution applications there is no significant loss of signal through relaxation on this timescale, but during an adiabatic sweep there is an appreciable variation in the instant at which a given group of spins is inverted, determined by their chemical shift.

In the majority of these experiments the frequency range of the adiabatic sweep is very large compared with the radiofrequency field intensity (expressed in frequency units), and to a good approximation we may neglect the relatively short time required to achieve a given degree of spin inversion. We may regard inversion as occurring at the point where the adiabatic frequency sweep passes through the chemical shift of a given group of spins. However, there will be a significant time difference for spin inversion of groups of spins with different chemical shifts.

Several authors (*16–19*) have studied the problem of compensating these timing variations when an adiabatic pulse is used to refocus chemical shift effects in a homonuclear spin-echo sequence. Here we address a different question—how to compensate the evolution due to spin–spin coupling when adiabatic pulses are used in heteronuclear spin-echo experiments. The present article proposes several new schemes that balance the evolution of spin–spin coupling caused by one adiabatic pulse against the opposing effect of a second adiabatic pulse, usually with the direction of frequency sweep reversed. We illustrate this use of ''compensating pairs'' of adiabatic pulses with reference to filtration experiments now widely used to simplify the high-field NMR spectra of biomolecules, and to adiabatic broadband decoupling techniques, but the principle is more general.

ISOTOPE FILTERS

It is often very useful to be able to separate proton signals of ^{13}C–H groups (where the single-bond coupling $^{1}J_{CH}$ is measured in hundreds of hertz) from all other proton signals. This has been called an ''isotope filter,'' in the sense that signals from protons directly attached to ^{13}C are retained, whereas signals from protons attached to ^{12}C are suppressed (*20, 21*). Such techniques afford a remarkable simplification

1090-7807/97 $25.00

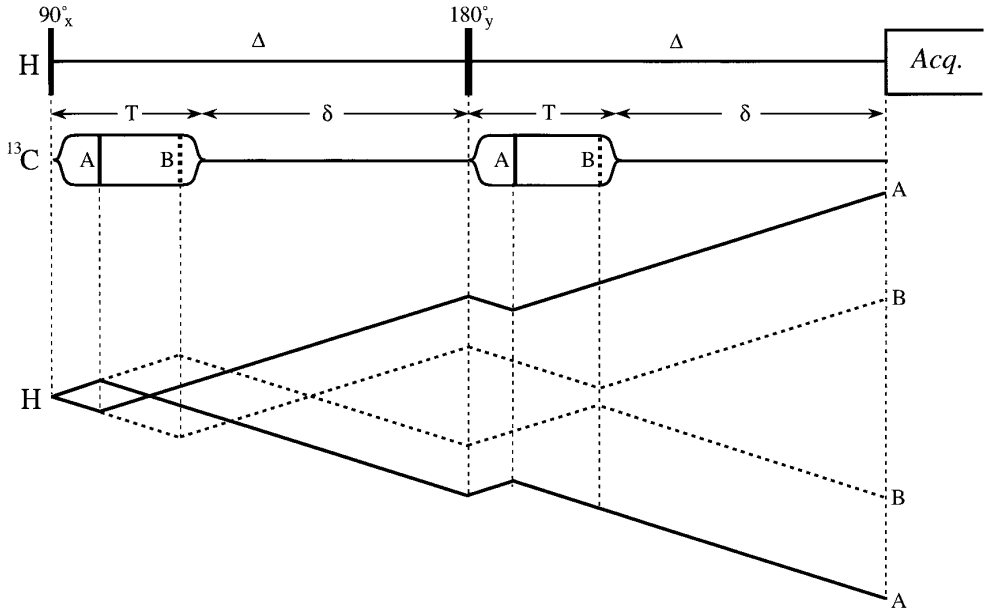

FIG. 1. The $^{13}C/^{12}C$ isotope filter experiment carried out with adiabatic sweeps in the *same* direction. The interval δ is set to the condition $1/(2J_{CH})$. The adiabatic sweeps are represented by the sausage-shaped profiles of duration T. The ^{13}C spins inverted during the early part of the sweep (''A'') exhibit an appreciably different phase evolution than those inverted later in the sweep (''B'').

in the proton spectra of isotopically enriched biomolecules. The separation is accomplished by a spin-echo difference method employing the sequence:

$$\begin{aligned} &\text{H spins} \quad 90^\circ_x - \delta - 180^\circ_y - \delta - \text{acquire}(\pm) \\ &^{13}\text{C spins} \quad 180^\circ\ (\text{on/off}), \end{aligned}$$

where $\delta = 1/(2J_{CH})$ and the 180°(^{13}C) pulse is only applied on odd-numbered scans, while the receiver phase is alternated. All proton magnetization vectors are left aligned along the $+y$ axis, except that during odd-numbered scans the additional 180° pulse induces $\pm\pi$ radians of precession for proton directly bound to ^{13}C, leaving them aligned along the $-y$ axis. The difference spectrum retains only the proton doublet from these ^{13}C molecules. Similar considerations apply to polarization transfer experiments derived from the INEPT sequence (*22*) except that the timing condition is then $\delta = 1/(4J_{CH})$. For simplicity we describe the operation of a $^{12}C/^{13}C$ isotope filter, although analogous considerations apply to a $^{14}N/^{15}N$ filter. Both are extensively used in biochemical NMR.

Unfortunately the range of ^{13}C chemical shifts that can be covered is limited by the effective bandwidth of the ^{13}C inversion pulse, and this may be inadequate, even if a composite 180° pulse is employed. Much wider bandwidths can be covered by adiabatic pulses, but then we must take care to cancel the blurring of the focus caused by the time shifts mentioned above.

The adiabatic pulse version of this experiment employs the sequence shown in Fig. 1, where the adiabatic sweeps (duration T) occupy an appreciable fraction of the spin-echo intervals Δ. On even-numbered scans, where the adiabatic pulses are omitted, the 180°_y proton pulse brings proton magnetization to a focus along the $+y$ axis of the rotating frame at time 2Δ. On odd-numbered scans, spin inversion is achieved by a pair of adiabatic pulses, but the exact instant of inversion is a function of the chemical shift of the ^{13}C spins. Two representative cases are considered, shown as a bold vertical bar for ''A'' spins inverted during the early part of the sweep, and by a dashed vertical bar for ''B'' spins inverted later in the sweep. It is convenient to illustrate this effect in terms of a proton phase evolution diagram (*23*). When both sweeps are in the same direction (Fig. 1) the phase divergence of protons attached to the ''A'' spins (full lines) exceeds that of protons attached to the ''B'' spins (dashed lines), giving a significantly different accumulated phase at time 2Δ. If spin inversion occurs at times $\alpha_A T$ and $\alpha_B T$ respectively (α_A and α_B being factors less than unity) then the accumulated phases may be written

$$\phi_A = \pm 2\pi J_{CH}[-\alpha_A T + (1 - \alpha_A)T + \delta] \qquad [1]$$

$$\phi_B = \pm 2\pi J_{CH}[-\alpha_B T + (1 - \alpha_B)T + \delta]. \qquad [2]$$

There is a consequent phase difference $\phi_A - \phi_B$ and in the general case, a blurring of the required focus.

The same sequence with a pair of opposed adiabatic

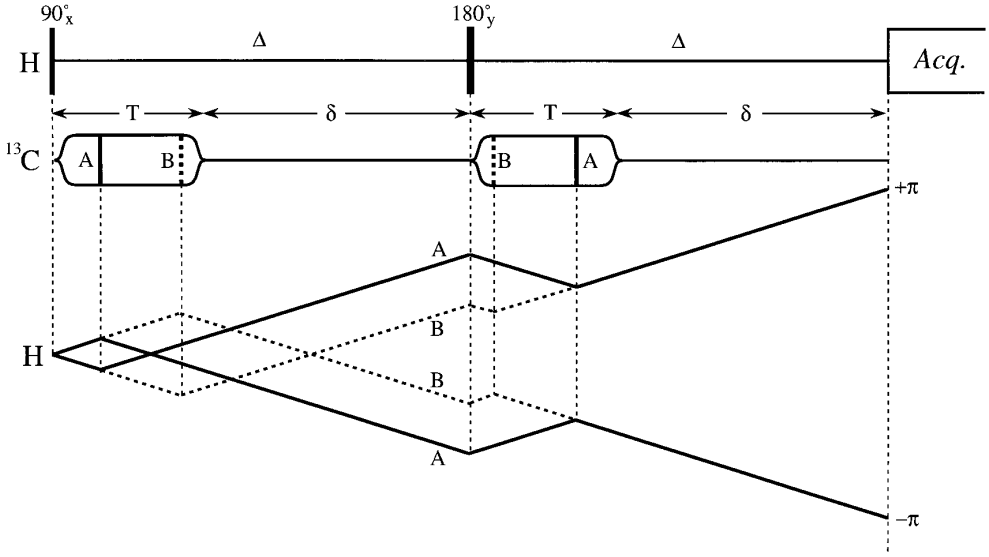

FIG. 2. The $^{13}C/^{12}C$ isotope filter experiment carried out with adiabatic sweeps in *opposite* directions. The interval δ is set to the condition $1/(2J_{CH})$. The adiabatic sweeps are represented by the sausage-shaped profiles of duration T. The ^{13}C spins inverted during the early part of the sweep (''A'') and those inverted later in the sweep (''B'') accumulate the same phase angles ($\pm\pi$ radians) at time 2Δ.

sweeps (Fig. 2) compensates for the variation in the time of spin inversion, generating the same total phase divergence in both cases

$$\phi_A = \phi_B = \pm 2\pi J_{CH}\delta. \qquad [3]$$

We see that one adiabatic pulse has cancelled the phase dispersion introduced by the other. There is no *net* phase evolution due to spin–spin coupling measured over the duration of the two adiabatic pulses. With δ is set equal to $1/(2J_{CH})$, the odd-numbered scans accumulate the desired

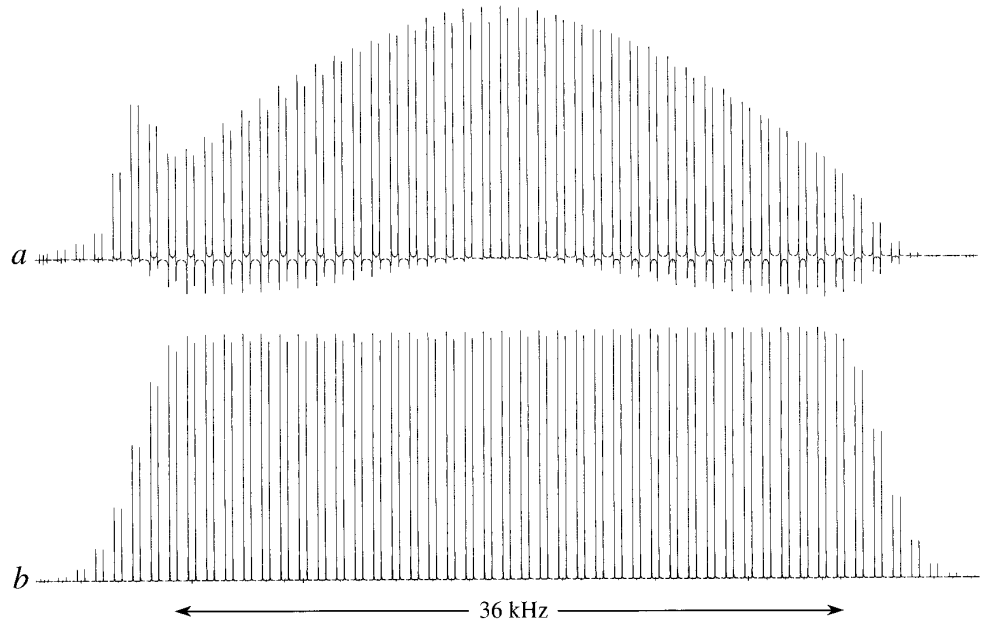

FIG. 3. Experimental $^{13}C/^{12}C$ isotope filter experiment (a) using the sequence of Fig. 1 with both adiabatic pulses in the same sense, and (b) using the sequence of Fig. 2 with the sweep directions opposed. The WURST-40 adiabatic pulse is used with a sweep duration of 3 ms, and an adiabaticity factor $Q_0 = 4$. The offset dependence (50 kHz in 1-kHz steps) illustrates the effect of ^{13}C chemical shifts at different points in the adiabatic sweep. Clearly the scheme with sweep directions opposed covers a wider effective bandwidth.

$\pm\pi$ radians of phase divergence at time 2Δ, aligning the proton vectors along the $-y$ axis. Subtraction of signals from odd and even scans retains only the response from directly bound ^{13}CH groups.

Figure 3 displays experimental results obtained for a sample of enriched methyl iodide (J_{CH} = 151 Hz), using WURST-40 adiabatic pulses (*6*) of duration T = 3.0 ms, with δ = 3.3 ms, $\gamma B_2(\max)/2\pi$ = 3 kHz, and an adiabaticity factor Q_0 = 4. When the two adiabatic sweeps are in the same direction (Fig. 3a), the performance is quite intolerant of offset (representing the ^{13}C chemical shift), inducing a serious falloff in amplitude of the detected proton resonances, and an appreciable phase dispersion. In contrast, operation with an opposed pair of adiabatic pulses (Fig. 3b) achieves a far wider effective bandwidth (36 kHz) with essentially uniform amplitudes. All coupled proton vectors reach a sharp focus along the $-y$ axis of the rotating frame.

The performance of a compensating pair of adiabatic pulses may be compared with that achieved with a simple rectangular pulse or a composite $90^\circ_x 180^\circ_y 90^\circ_x$ pulse (*2*). Since it is unrealistic to compare hard radiofrequency pulses and adiabatic passage methods at the same *mean* radiofrequency power, the experiments were all performed at the same *maximum* radiofrequency intensity, $\gamma B_2(\max)/2\pi$ = 5.0 kHz. The rectangular pulses, which had a duration 100 μs, were clearly very inefficient, displaying a sinc-like frequency-domain profile for the proton response (Fig. 4a). The $90^\circ_x 180^\circ_y 90^\circ_x$ composite pulses, with a duration of 200 μs, fared rather better, covering a ^{13}C offset range of 10 kHz with reasonable uniformity (Fig. 4c). Interestingly, an opposed pair of 1-ms hyperbolic secant pulses with the same $B_2(\max)$ had an even narrower effective bandwidth (6 kHz) but better uniformity (Fig. 4b). The self-compensating pair of adiabatic pulses, based on WURST-20 with a duration of 1 ms, proved far superior, covering an offset range of 32 kHz with commendable uniformity (Fig. 4d).

Self-compensating pairs of adiabatic pulses afford a method for ''neutralizing'' J evolution during a chosen interval of a refocusing experiment, since there is no *net* divergence due to spin–spin coupling when measured over the two T intervals. This could be useful in certain ''round-trip'' polarization transfer experiments (HSQC) involving ^{13}C and ^{15}N simultaneously:

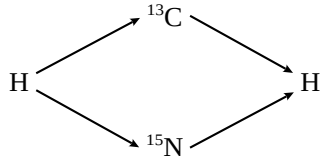

The neutral period during which J evolution is suppressed could be exploited to compensate for the difference between the magnitudes of ^{13}CH and ^{15}NH coupling constants (*24, 25*).

COMPENSATION FOR A VARIATION IN J_{CH} COUPLINGS

In practical situations we are often faced with the problem of operating an isotope filter when there is a natural distribution of the magnitudes of the heteronuclear spin–spin coupling constants. Then no single choice of the δ delay will bring all proton vectors to the $\pm\pi$ condition (even if a hard 180° pulse is used as the agent for spin inversion). Fortunately there is a rough proportionality between ^{13}C chemical shifts and the coupling constants $^1J_{CH}$. For example, aromatic ^{13}C nuclei have $^1J_{CH}$ in the range 160–180 Hz, ^{13}C attached to nitrogen or oxygen has $^1J_{CH}$ of about 140 Hz, while ^{13}C in a methyl group has $^1J_{CH}$ of about 125 Hz. Thus, by judicious choice of the adiabatic sweep rate we can play off the phase deviations generated by the ^{13}C chemical shifts against those caused by the mismatch of the timing with respect to $^1J_{CH}$, provided we sweep the frequency in the right sense.

There are two alternative pulse sequences for these J-compensated experiments. The ''single sweep'' experiment may be written

$$\begin{array}{lll} \mathrm{H} & 90^\circ - \delta_1 - 180^\circ - & -\delta_2 - \text{acquire} \\ {}^{13}\mathrm{C} & a \,|\, b, & \end{array}$$

where the symbol ''|'' represents the point at which spin inversion is achieved during the adiabatic pulse. The adiabatic sweep duration $T = a + b$; spins inverted at the very start of the sweep have $a = 0$, while those inverted at the very end of the sweep have $b = 0$. The refocusing condition is now

$$\delta_1 = a + b + \delta_2 = 2c/J_{CH}, \qquad [4]$$

where the constant c = 0.25 for heteronuclear single-quantum correlation (HSQC) experiments, and c = 0.5 for isotope filter experiments. We assume that J_{CH} varies linearly with ^{13}C chemical shift (ν) so that

$$J_{CH} = \nu \frac{dJ_{CH}}{d\nu} + \text{const.} \qquad [5]$$

We sweep from low to high radiofrequency (high to low field), corresponding to the direction $J(\min)$ to $J(\max)$. Thus $a = 0$, $b = T$ for a group with $J(\min)$, whereas $a = T$, $b = 0$ for a group with $J(\max)$. We set

$$\delta_1 = c/J(\min) \text{ and } \delta_2 = c/J(\max). \qquad [6]$$

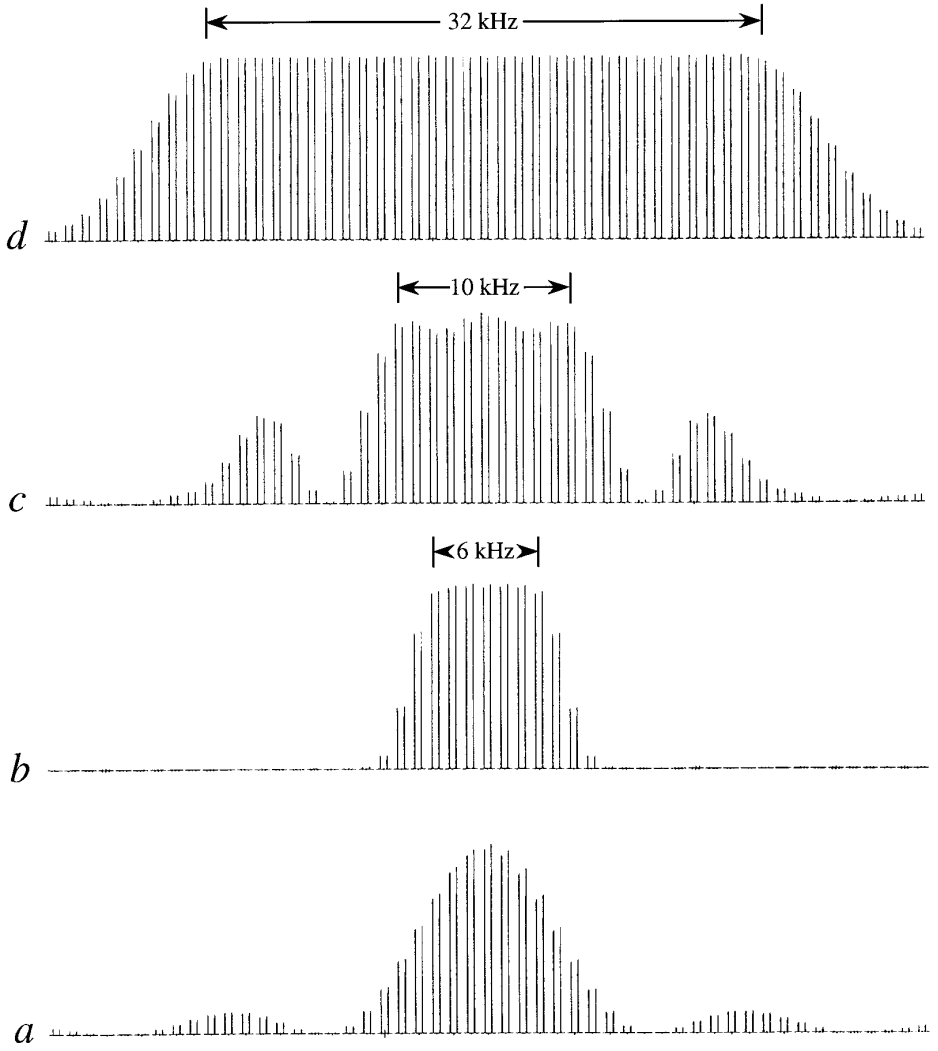

FIG. 4. Comparison of the effective bandwidths achieved in the isotope filter experiment with (a) a rectangular 180° pulse, (b) an opposed pair of 1-ms hyperbolic secant pulses, (c) a $90^\circ_x 180^\circ_y 90^\circ_x$ composite pulse, and (d) an opposed pair of 1-ms WURST-20 adiabatic pulses. All pulses were limited to the same maximum radiofrequency level $\gamma B_2(\max)/2\pi = 5.0$ kHz.

This permits the evaluation of the optimum sweep duration for J compensation:

$$T_{\text{opt}} = \delta_1 - \delta_2 = \frac{c}{J(\min)} - \frac{c}{J(\max)} = c\,\frac{J(\max) - J(\min)}{J(\max)J(\min)}. \qquad [7]$$

Note that the T_{opt} is independent of spectrometer frequency. Had we chosen to employ the alternative arrangement

H $\quad 90°-\delta_2-\quad\quad -180°-\delta_1-$acquire

^{13}C $\quad\quad\quad b\,|\,a$

the sweep direction would need to be reversed.

Consideration of the phase evolution diagram of Fig. 1 makes it clear that if the *A* spins had a slower divergence due to $^1J_{\text{CH}}$ than the *B* spins, then a judicious choice of *T* would allow both phase trajectories to reach the same focus at time 2Δ. We may therefore formulate an alternative (''double-sweep'') mode:

H $\quad 90°-\quad\quad -\delta-180°-\quad\quad -\delta-$acquire

^{13}C $\quad\quad a\,|\,b\quad\quad\quad\quad a\,|\,b$

which has the refocusing condition

$$\delta + a + b = c/(J_{\text{CH}}). \qquad [8]$$

With the same considerations as above [$a = 0$ for $J(\min)$; $b = 0$ for $J(\max)$], we obtain

$$\delta + T = c/J(\min) \text{ and } \delta - T = c/J(\max) \quad [9]$$

$$T_{opt} = \frac{c}{2J(\min)} - \frac{c}{2J(\max)} = \frac{c}{2}\frac{J(\max) - J(\min)}{J(\max)J(\min)}. \quad [10]$$

Note that for this pulse sequence with two adiabatic sweeps, the optimum sweep duration is halved, making it more difficult to fulfil the adiabatic condition. Had we chosen to adopt the alternative arrangement

H	$90°-\delta-$		$-180°-\delta-$	acquire
^{13}C		$b \mid a$		$b \mid a$

the sweep direction would need to be reversed.

To get an idea of practical parameters in this experiment, we might consider a methyl group with a ^{13}C chemical shift of 20 ppm and $^1J_{CH}$ = 120 Hz, and an aromatic site with a ^{13}C chemical shift of 140 ppm and $^1J_{CH}$ = 160 Hz. Suppose we decide to employ an effective spin-inversion bandwidth of 150 ppm. The adiabatic sweep rate should satisfy the condition

$$\frac{dJ_{CH}}{d\nu} = \frac{40 \text{ Hz}}{120 \text{ ppm}}. \quad [11]$$

We would therefore implement an adiabatic sweep from 5 to 155 ppm with J_{min} = 115 Hz and J_{max} = 165 Hz, and if we employ the single-sweep method (where $c = 0.5$) then the optimum sweep duration would be T_{opt} = 1.32 ms (from Eq. [7]). For the double-sweep method T_{opt} would be 0.66 ms (from Eq. [10]).

We take as illustrative example a sample consisting of a mixture of methyl iodide, which has J_{CH} = 151 Hz, and $^{13}CH_3PO(OCH_3)_2$, which has J_{CH} = 129 Hz. The two ^{13}C resonances are 33.1 ppm apart. Ordinarily, with the sequence of Fig. 2, the discrepancy in coupling constants would mean that an isotope filter experiment with a refocusing delay δ tuned to J_{CH} = 129 Hz would be incorrectly set for the other coupling (J_{CH} = 151 Hz), inducing a serious phase error in the proton response from methyl iodide (Fig. 5a). However, when we apply adiabatic sweeps in the same sense, and select the appropriate sweep rate (-44.6 MHz s^{-1}) the two responses are both recorded in phase (Fig. 5b). Note the importance of sweeping in the direction from low to high field; when the sweep direction is reversed (Fig. 5c) the phase distortion on the methyl iodide response is far worse. With only two chemical sites this compensation can be made exact, but in the general multisite case it can only be approximate, relying on the roughly linear relationship between ^{13}C chemical shifts and the corresponding magnitudes of $^1J_{CH}$.

When a short duration radiofrequency pulse is applied at the same time as a second pulse of much longer duration, the accepted practice is to synchronize the centers of the two pulses, on the grounds that this is the only symmetrical arrangement (*26*). It turns out that this is not the optimum arrangement when there is a range of spin–spin coupling constants to be refocused by an adiabatic pulse (*27*). Provided that there is an approximately linear relationship between the ^{13}C shifts and the corresponding $^1J_{CH}$ coupling constants, and with the correct choice of the adiabatic sweep rate and sweep direction, focusing can be achieved by starting the adiabatic pulse immediately *after* the hard 180° pulse. This is illustrated in Fig. 6, where one group of ^{13}C spins (''*A*'') with a smaller coupling constant $^1J_{CH}$ is inverted early in the adiabatic sweep, whereas a second group of ^{13}C spins (''*B*'') with a larger coupling constant is inverted later in the sweep. The phase evolution diagram demonstrates how proton magnetization from both groups can be brought to a focus along the $-y$ axis ($\pm\pi$ radians precession) if the adiabatic sweep duration is correctly chosen. In contrast, an adiabatic pulse symmetrically disposed about the hard 180° pulse does *not* achieve compensation across the range of $^1J_{CH}$ values because a crossover of the *A* and *B* phase trajectories is essential for refocusing.

REFOCUSING DURING THE EVOLUTION PERIOD OF A TWO-DIMENSIONAL EXPERIMENT

It is sometimes necessary to refocus the divergence of proton vectors due to coupling to ^{13}C during the evolution period of a two-dimensional experiment by means of a spin inversion pulse applied to ^{13}C. In high-field NMR spectrometers this requires that the spin inversion be effective over a wide chemical shift range. If an adiabatic inversion pulse is used for this purpose, the appreciable sweep duration can give rise to refocusing errors. The offending time-shifts introduced by one adiabatic pulse can be compensated by an identical pulse at the end of the evolution period. In this case the two adiabatic sweeps have the same sense. Consider three groups of ^{13}C spins with chemical shifts *a*, *b*, and *c* (Fig. 7). The *a* spins are inverted early in the adiabatic sweep and would normally reach a focus before the end of the evolution period, but because they are inverted again early in the second adiabatic sweep, the two proton vectors are brought to a focus at the right instant. In a similar manner, the *b* spins, inverted near the middle of the sweep, are reinverted near the middle of the second sweep and also reach the correct focus point. An analogous compensation applies to the *c* spins which are inverted late in the adiabatic sweep. Note that the first adiabatic pulse terminates at the midpoint of the evolution period t_1. The operation is similar to the chemical shift refocusing scheme already mentioned (*18*).

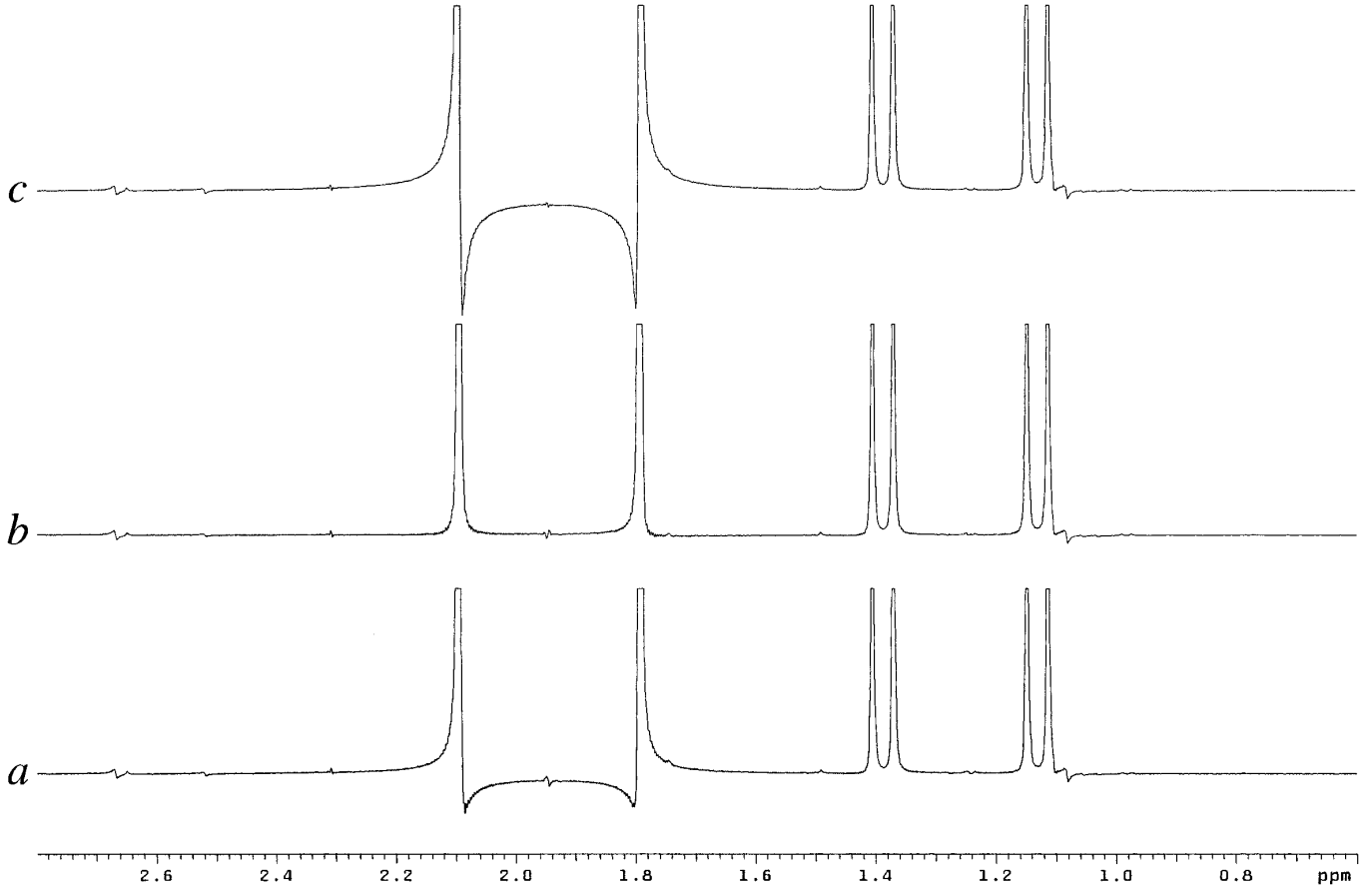

FIG. 5. The isotope filter experiment performed on a mixture of $^{13}CH_3I$ (J_{CH} = 151 Hz) and $^{13}CH_3PO(OCH_3)_2$ (J_{CH} = 129 Hz) to illustrate how a variation in coupling constants can be accommodated. (a) An opposed pair of adiabatic sweeps (Fig. 2) with δ = 3.88 ms (appropriate for J_{CH} = 129 Hz) generates an appreciable phase error on the proton response from methyl iodide (left). (b) The same sequence except that both ^{13}C adiabatic sweeps are in the same sense (Fig. 1) and the sweep rate has been optimized, giving pure absorption for both responses. (c) As (b) but with both sweeps in the wrong direction, exacerbating the phase error. All signals have been truncated in order to highlight the dispersion contributions.

CYCLING SIDEBANDS IN BROADBAND DECOUPLING

The recent introduction of adiabatic fast passage methods for heteronuclear decoupling in liquid-phase high-resolution NMR spectroscopy permits extremely wide chemical shift ranges to be covered without undue sample heating (*3–15*). The principal remaining practical problem is the spurious modulation that appears on the time-domain signals at the cycling frequency and at certain harmonics and subharmonics. After Fourier transformation this appears as cycling sidebands (*28*) in the decoupled spectrum, and these could interfere with the detection of very weak signal components. These artifacts are more obtrusive the lower the radiofrequency level (B_2) used for decoupling (*8*). If high detection sensitivity is to be achieved, it is essential to reduce cycling sidebands to a very low level. For the purposes of illustration we examine this question in the context of WURST decoupling (*6, 8, 10, 12*) of ^{13}C with observation of the proton spectrum, although the same treatment is applicable to most adiabatic decoupling schemes.

During adiabatic decoupling with no ''windows'' between the decoupler pulses, the cycling sidebands fall into three main categories (*8*). The *principal* sidebands flank the decoupled resonance at $\pm 1/T$ (hertz) where T is the duration of the adiabatic pulse. The amplitude and phase of these sidebands depend on the position of the chemical shift of the ^{13}C spins with respect to the adiabatic sweep. If the ^{13}C spins are inverted near the center of the sweep then the principal proton sidebands are relatively strong and in pure absorption, but if the ^{13}C chemical shift lies nearer the ends of the sweep the sidebands show increasing dispersion-mode contributions. The picture is considerably simplified if we combine the spectra from two scans taken with opposite directions of the decoupler frequency sweep. Then the dispersion contributions cancel and the intensity of the principal sidebands follows the pattern illustrated in Fig. 8a, being

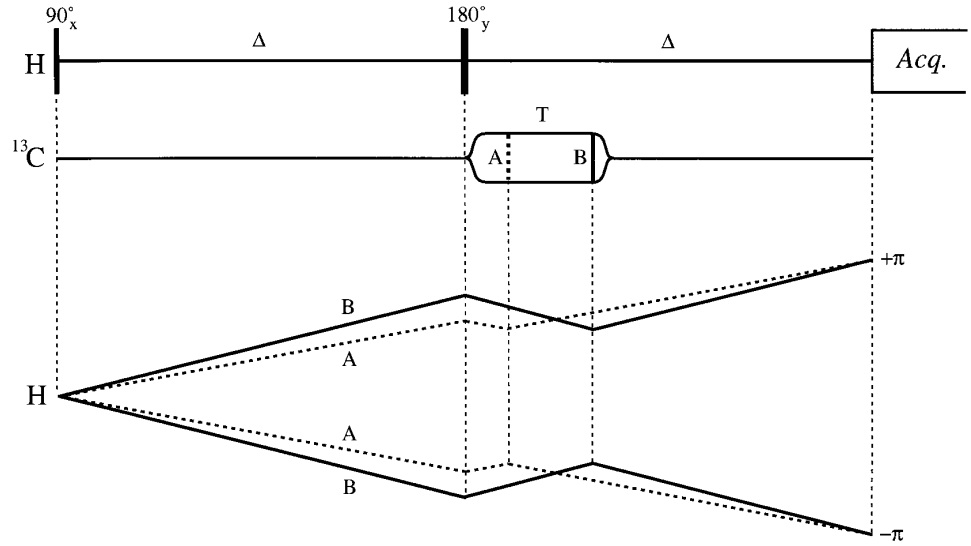

FIG. 6. Phase evolution diagram illustrating how the proton signals from two different ^{13}CH groups (''*A*'' and ''*B*'') can be refocused to give $\pm\pi$ radians of phase divergence. Group *A* has the smaller coupling constant and has the ^{13}C spins inverted early in the adiabatic sweep (dashed lines), whereas group *B* has the larger coupling constant and has the ^{13}C spins inverted later in the sweep (full lines). The adiabatic sweep rate (and direction) must be correctly chosen, and success in the general case relies on a roughly linear relationship between the ^{13}C chemical shifts and the magnitudes of the ^{13}CH coupling constants.

most prominent when the decoupled spin has a chemical shift near the center of the adiabatic sweep, passing through nulls at about $\frac{1}{4}$ and $\frac{3}{4}$ of the sweep width, and appearing weaker and inverted for chemical shifts near the extremities of the adiabatic sweep.

The principal cycling sidebands arise from a spurious modulation that takes the form of a connected sequence of short sections of a cosine wave. Consequently the Fourier spectrum contains components at $\pm n/T$ Hz where $n = 1, 2, 3, \ldots$ etc., becoming progressively weaker as n increases.

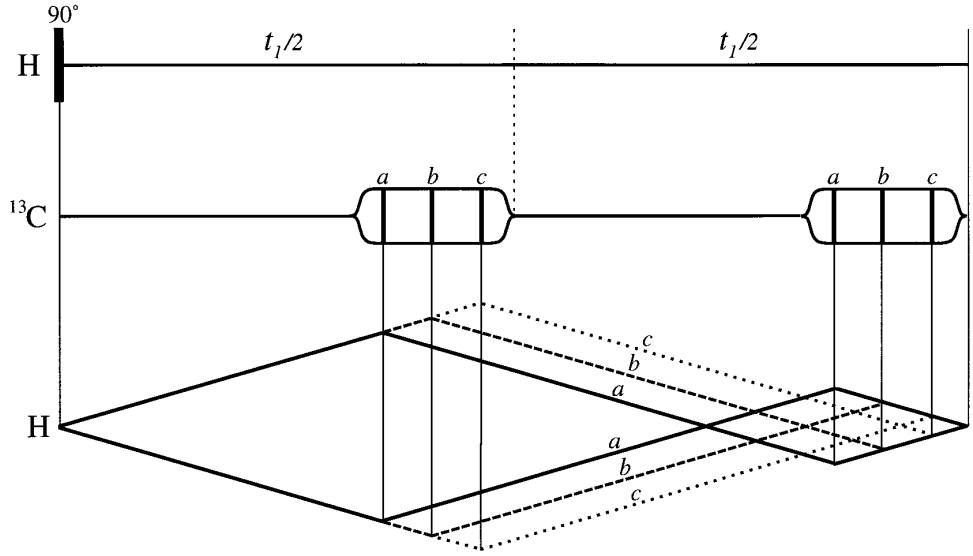

FIG. 7. Phase evolution diagram for the proton vectors during the evolution period (t_1) of a two-dimensional experiment in which the coupled ^{13}C spins are inverted by an adiabatic pulse of appreciable duration. Three groups of ^{13}C spins are considered, with chemical shifts *a*, *b*, and *c*. Normally the proton vectors would reach a focus too early, but the second adiabatic pulse with the *same* sweep direction compensates these time-shifts and brings the proton vectors of all three groups to an exact focus at the end of the evolution period.

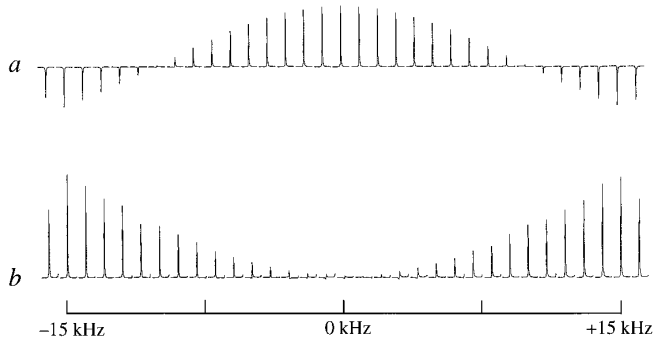

FIG. 8. Principal (a) and subharmonic cycling sidebands (b) recorded during adiabatic decoupling and displayed as a function of the chemical shift of the decoupled spins measured with respect to the center of the frequency sweep. Dispersion mode contributions have been eliminated by adding two scans obtained with opposite adiabatic sweep directions. Note that the algebraic sum of the corresponding intensities in (a) and (b) is essentially constant within the operating range.

We shall see that these higher harmonics do not necessarily disappear when the principal cycling sidebands are suppressed.

The second kind are the *subharmonic* sidebands, generated from spurious modulation at $\pm 1/(2T)$ Hz. Once the dispersion contributions have been eliminated by combining results from two sweep directions, the subharmonic sidebands follow the pattern illustrated in Fig. 8b, with high intensity for ^{13}C chemical shifts near the edges of the adiabatic sweep and negligible intensity near the middle (*8*). In fact the intensities of principal and subharmonic sidebands are complementary, giving an essentially constant algebraic sum, independent of chemical shift of the ^{13}C spins.

This interplay between the intensities of the principal and subharmonic sidebands is vividly illustrated in a phase evolution diagram (*23*) in which the divergence of proton vectors due to J_{IS} is refocused as the adiabatic sweep passes through the relevant ^{13}C chemical shift (represented by a bold vertical bar). Figure 9a demonstrates that ^{13}C spins that are inverted near the middle of the adiabatic sweep show a cycling modulation of the proton signal that is predominantly at $1/T$ Hz, whereas ^{13}C spins that are inverted near the edge of the sweep generate a modulation that is mainly at $1/(2T)$ Hz (Fig. 9c). Any practical sideband suppression scheme must take these variations into account.

The third kind are the *inner* cycling sidebands (*8*) which appear at offsets of $\pm 1/(pT)$ Hz, where p is the number of adiabatic pulses in the cycle or supercycle. Consequently they lie close to the decoupled resonance line in the observed spectrum. Inner cycling sidebands tend to be rather weak under normal decoupling conditions, and become less obtrusive the more faithfully the adiabatic condition is satisfied.

We concentrate on the suppression of the principal cycling sidebands at $1/T$ Hz because the subharmonic and inner cycling sidebands are readily reduced by other methods (*18*). With the schemes described above, where the adiabatic sweep rate and direction are chosen so as to compensate for a range of ^{13}CH coupling constants, the subharmonic sidebands are strongly attenuated. The distribution of intensities is no longer that illustrated in Fig. 8b, with strong sidebands near the edges of the adiabatic sweep. Excessive phase divergence due to ^{13}C chemical shift effects is balanced by the opposing influence of the variation in ^{13}CH coupling constants.

With adiabatic decoupling, the principal sidebands cannot be reduced simply by desynchronizing the decoupler timing with respect to the sampling operation; this only alters the relative intensities of the principal and subharmonic sidebands, rendering any averaging method ineffective. Again we may use a phase evolution diagram (Fig. 10) to make this point. A straightforward time-shift of the decoupler cycling with respect to proton acquisition perturbs the relative amplitudes of the principal and subharmonic cycling modulations.

Efficient suppression requires a more sophisticated time-shifting scheme that maintains a constant ratio between the intensities of the principal and subharmonic sidebands. One solution to this problem (''ECO-WURST'') has already been implemented in the form of bilevel decoupling, where the decoupler is operated at a high level for a short variable interval, during which the cycling modulation is negligible,

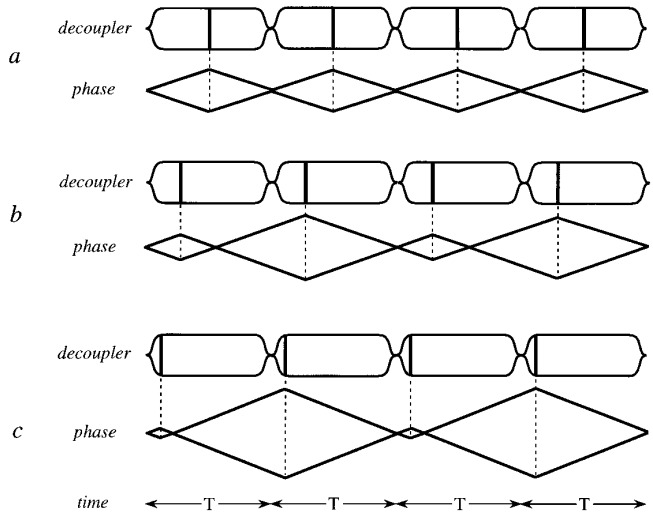

FIG. 9. Phase evolution diagram showing the spurious cycling modulation predicted for adiabatic decoupling. There are two main modulation components, one at $1/T$ Hz (principal) and the other at $1/(2T)$ Hz (subharmonic). Their relative intensities depend on the chemical shift of the ^{13}C spins (represented by bold vertical bars) in relation to the adiabatic sweep (represented by the sausage-shaped WURST profile). For a ^{13}C chemical shift near the middle of the sweep (a) the principal component dominates (cf. Fig. 8a), whereas for a ^{13}C chemical shift near the beginning or end of the sweep (c) the subharmonic component dominates (cf. Fig. 8b).

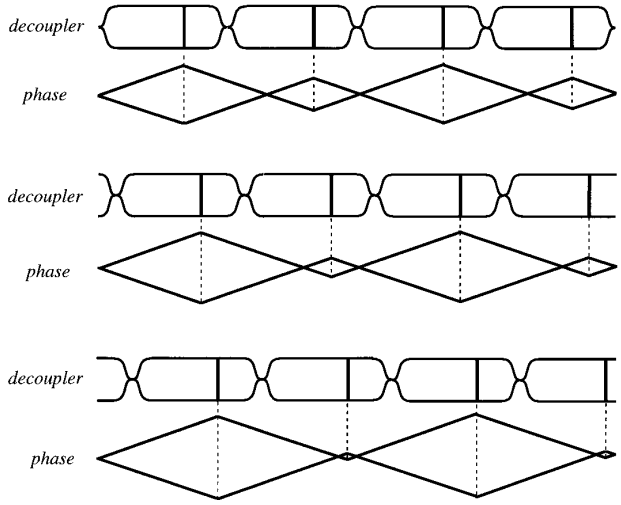

FIG. 10. Phase evolution diagram to show that desynchronizing the ^{13}C decoupler pulses with respect to the proton signal acquisition alters the relative intensities of the principal and subharmonic modulation frequencies. This means that these undesirable modulations cannot be effectively cancelled by averaging several scans.

followed by signal acquisition with normal low-level decoupling (*29*). Unfortunately this method may not be suitable for some high-resolution spectrometers. We describe here an alternative procedure (''ECHO-WURST'') that is simpler to implement and which avoids the use of high-level radiofrequency irradiation.

In its simplest form the new procedure accumulates decoupled spectra obtained with different phase shifts of the cycling modulation. The key to the operation is the use of a sequence of two identical adiabatic sweeps in opposite directions, so that ^{13}C spins with a chemical shift in the first half of the sweep range during the first pass find themselves in the second half of the range during the second pass. The first two adiabatic sweeps have duration $\tau < T$ and are followed by the normal decoupler sweeps of duration T, all in the same sense.

Proton signal acquisition is delayed by a *fixed* interval 2Δ, and a spin-echo sequence introduces a refocusing pulse at time Δ:

$$90^\circ_x - \Delta - 180^\circ_y - \Delta - \text{acquire (protons)}.$$

This ensures that proton chemical shifts are always refocused at time 2Δ, whereas the divergence due to J_{CH} can be varied by systematically displacing the timing of the second adiabatic pulse. The appropriate phase evolution diagram is shown in Fig. 11 for two different timings. The first adiabatic pulse (duration τ) is fixed at the midpoint of the first Δ interval, but the second adiabatic pulse (duration τ, but reversed in sense) can be shifted in time in order to generate the required phase shift of the modulation. The variable interval is δ'. For simplicity we may take the proton chemical shift to be at resonance (it would in any case be

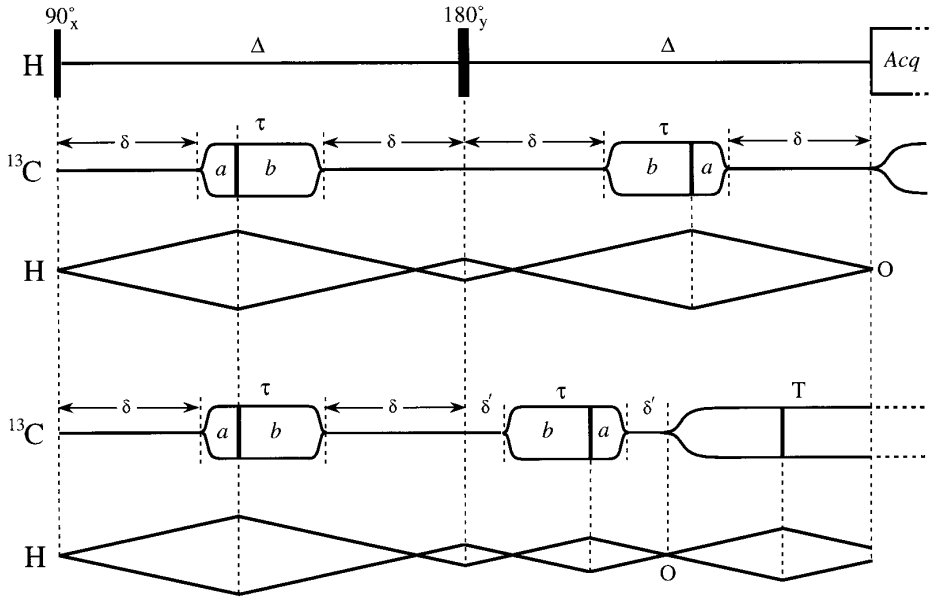

FIG. 11. Shifting the phase of the principal cycling modulation in the ECHO-WURST scheme. Two fast adiabatic sweeps are employed, both of duration τ but in opposite senses. The subsequent decoupler sweeps have a longer duration T. The proton chemical shift is refocused by the spin-echo sequence (top). We consider ^{13}C spins with an arbitrary chemical shift (represented by the bold vertical bar) inverted after a delay a, where $a + b = \tau$. By varying δ', the focus point O can be displaced, shifting the phase of the modulation detected during the acquisition period. In the lower diagram this time shift is $-T/2$, giving a phase shift of 180°. Addition of the two scans greatly attenuates the modulation.

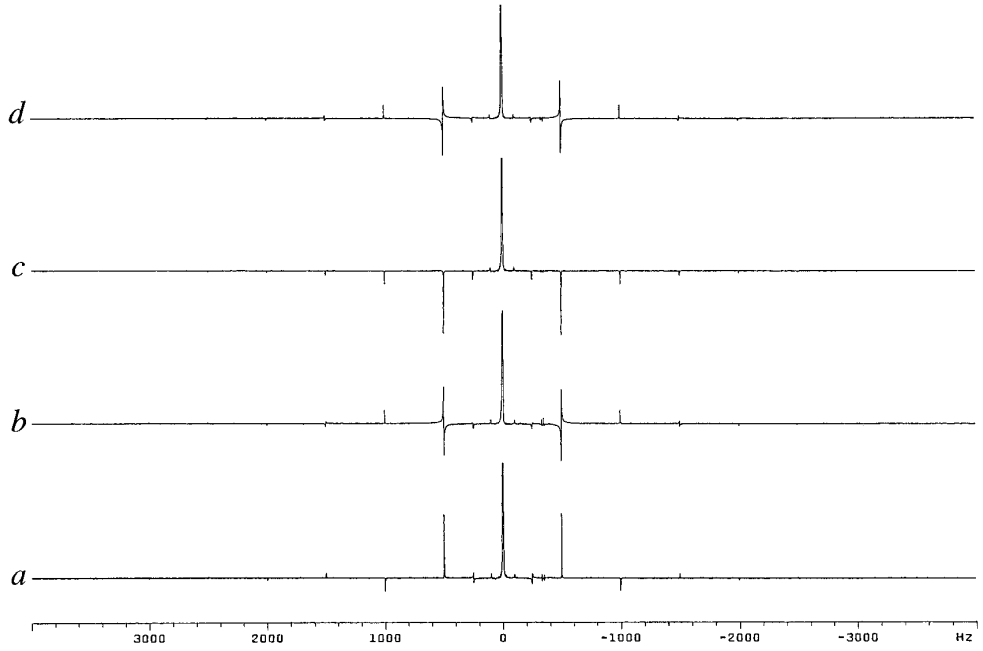

FIG. 12. The 500-MHz proton spectrum of methyl iodide decoupled from ^{13}C with the ECHO-WURST adiabatic scheme with time shifts of (a) 0, (b) $T/4$, (c) $T/2$, and (d) $3T/4$ ms. The cycling sidebands are at $\pm 500n$ Hz, where n is the order. Addition of traces (a) and (c) cancels all the odd-order cycling sidebands, leaving only those with $n = 2, 4, 6, \ldots$, etc. Addition of all four traces also cancels the sidebands with $n = 2, 6, 10, \ldots$, etc., leaving only the sidebands for $n = 4, 8, 12, \ldots$, etc., which are inherently very weak indeed.

refocused by the 180° pulse). We fix our attention on an arbitrary ^{13}C chemical shift which is inverted at a point a of the adiabatic sweep ($a + b = \tau$) and follow the phase evolution $\Delta\phi$ of the proton doublet. For the general case, where $\delta \neq \delta'$, we have

$$\Delta\phi = \pm\pi J_{IS}[\delta + a - b - \delta + \delta' + b - a - \delta'] = 0. \quad [12]$$

This ensures that the cycling modulation is brought to a focus (point O) whatever the ratio δ/δ'. Consequently, by starting the normal decoupling at this variable focus, ECHO-WURST shifts the phase of the detected cycling modulation. All subsequent adiabatic sweeps (during signal acquisition) are identical, setting up a regular refocusing regime in which the larger and smaller phase excursions alternate in time, with a fixed ratio of the intensities of the principal and subharmonic modulation components, independent of the choice of δ'. (Note the practical point that the normal practice of resetting the decoupler at the start of signal acquisition must be disabled for this application.)

Sideband Intensities

In the absence of any ^{13}C inversions, the proton signal at resonance (and neglecting relaxation) is modulated simply as $\cos(\pi J_{CH}t)$. Introduction of ^{13}C inversions converts this wave into a sequence of small arcs which can be represented by a Fourier series (*30*) in which all the sine terms are zero because the modulation is symmetric in time:

$$M_y(t) = \tfrac{1}{2}A_0 + \sum_{n=1}^{\infty} A_n \cos(2\pi nt/T). \quad [13]$$

The centerband (the decoupled proton resonance) has the intensity

$$A_0 = \frac{1}{T}\int_{-T/2}^{T/2} \cos(\pi Jt)dt = 2\sin(\pi JT/2)/\pi JT. \quad [14]$$

Assuming that the ^{13}C spins are inverted at the center of the adiabatic sweep, the sideband intensities can be found from the higher-order Fourier coefficients

$$A_n = \frac{2}{T}\int_{-T/2}^{T/2} \cos(\pi Jt)\cos(2\pi nt/T)dt = \frac{-4JT}{\pi[4n^2 - (JT)^2]}\sin(\pi JT/2)\cos(n\pi). \quad [15]$$

It follows from Eq. [15] that the odd-order sidebands ($n =$

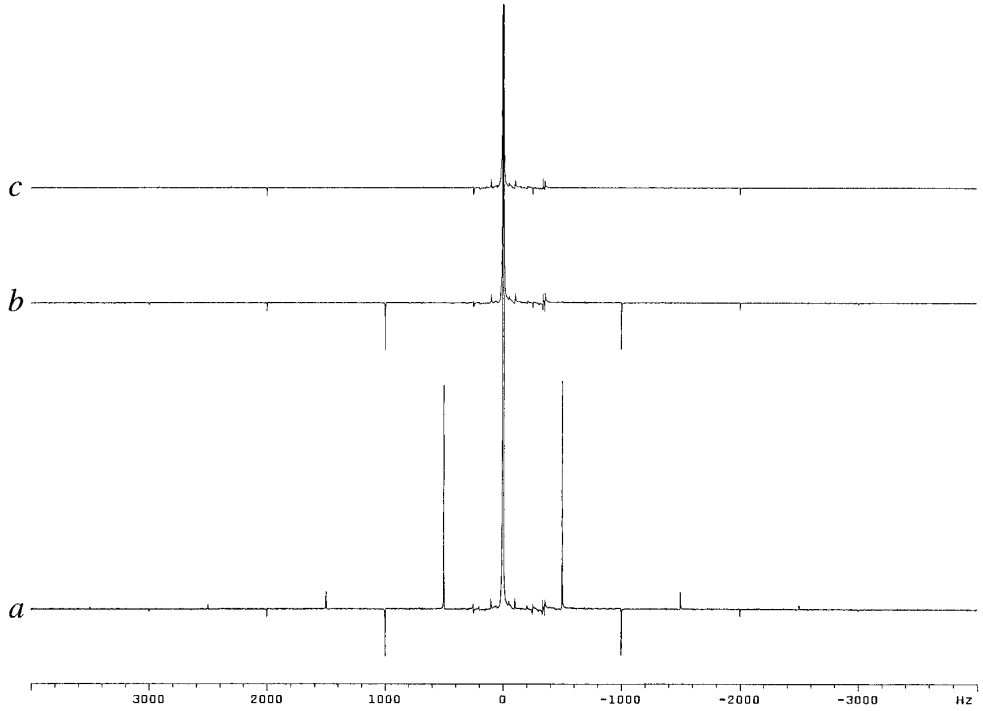

FIG. 13. Reduction of the principal cycling sidebands in the 500-MHz proton spectrum of ^{13}C-enriched methyl iodide with WURST-40 decoupling. (a) After a single scan the principal sidebands ($n = 1$) at ±500 Hz represent 2% of the height of the decoupled line, and weaker sidebands for $n = 2$, 3, 4, 5, 6, and 7 are also visible. (b) After two scans with the ECHO-WURST scheme, all the odd-order sidebands have been suppressed, leaving only the negative sidebands for $n = 2$, 4, and 6. (c) After four scans only the negative sidebands for $n = 4$ are discernible; they have an intensity 0.06% of the decoupled peak. All four spectra have the same vertical scale, with the decoupled resonance truncated.

1, 3, 5, . . .) have the opposite sense to the even-order sidebands ($n = 2, 4, 8, \ldots$).

ECHO-WURST shifts the modulation by half the duration of the pulse ($T/2$) so that the final cosine term in Eq. [15] vanishes and all the sidebands are negative:

$$A_n' = \frac{2}{T}\int_0^T \cos(\pi Jt + \pi JT/2)\cos(2\pi nt/T)dt$$

$$= \frac{-4JT}{\pi[4n^2 - (JT)^2]}\sin(\pi JT/2). \qquad [16]$$

Consequently, coherent addition of signals corresponding to these two cases (Eqs. [15] and [16]) suppresses all the odd-order sidebands:

$$A_n + A_n' = \frac{-4JT}{\pi[4n^2 - (JT)^2]} \times \sin(\pi JT/2)[1 + \cos(n\pi)]. \qquad [17]$$

The first sideband ($n = 1$) is by far the most important and is cancelled by this procedure. In actual fact the spin inversions are not instantaneous, causing the discontinuities in the proton modulation to be rounded off, with the result that the higher-order sidebands are less intense than predicted by the Fourier series expansion. It can be shown that averaging four scans with time shifts 0, $T/4$, $T/2$, and $3T/4$ also cancels certain even-order sidebands ($n = 2, 6, 10, \ldots$, etc.), and we are left only with the extremely weak sidebands corresponding to $n = 4, 8, 12, \ldots$, etc.

Experimental Results

The changes in sense of the principal cycling sidebands and their harmonics is illustrated in Fig. 12 for a four-step sequence where the time shift is 0, $T/4$, $T/2$, and $3T/4$ ms. Note that addition of two traces, for example 12a and 12c, cancels the principal sidebands (2.0% of the decoupled line) and the third harmonics, but leaves the second harmonic, which has an intensity equal to 0.4% of the decoupled resonance. As predicted above, addition of all four traces cancels the first, second, and third harmonics but leaves the very weak fourth harmonic, which is negative-going in all four traces. Higher harmonics are so weak that they can be safely neglected, although the sequence could be extended to eradicate them if necessary.

Figure 13a shows the typical level of cycling sidebands

in the decoupled proton spectrum of methyl iodide with WURST-40 decoupling of ^{13}C. Conditions were deliberately chosen so that the principal cycling sidebands at ± 500 Hz were quite intense (2% of the height of the decoupled line) and higher-order sidebands up to $n = 7$ were visible. When the normal proton free induction decay is added to that from a second scan with a time-shift of the cycling modulation of $T/2$ ms, all the odd-order cycling sidebands (which were positive-going) disappear (Fig. 13b) leaving only those for n = 2, 4, 6, . . . , etc. When four scans are accumulated with time-shifts of 0, $T/4$, $T/2$, and $3T/4$ ms, the harmonics $n = 2$ and $n = 6$ are suppressed, leaving just the weak negative-going sidebands for $n = 4$ (Fig. 13c). These have approximately 0.06% of the intensity of the decoupled resonance. Clearly ECHO-WURST decoupling may be used in situations where there are very weak signals that must be detected (for example, weak proton NOESY cross peaks) without danger of interference from decoupling sidebands.

CONCLUSIONS

Spin inversion by adiabatic rapid passage involves a relatively long sweep duration (milliseconds), and consequently the instant at which a given group of spins is inverted is a function of the chemical shift. This can introduce an undesirable phase dispersion in proton spin-echo experiments involving spin inversion of ^{13}C (or ^{15}N) by adiabatic rapid passage. A simple solution to this problem employs a self-compensating pair of adiabatic pulses, balancing the time-shift introduced during one adiabatic sweep against an equal but opposite shift generated by the second sweep. This promises to have important applications in high-field NMR of isotopically enriched biomolecules since the substitution of hard radiofrequency pulses by adiabatic pulses greatly increases the effective bandwidth for spin inversion. The technique has been extended to accommodate a range of $^1J_{CH}$ coupling constants, by exploiting the roughly linear relationship between $^1J_{CH}$ and the ^{13}C chemical shift. A second important application addresses the problem of suppressing cycling sidebands in broadband adiabatic decoupling experiments; it is demonstrated experimentally that the introduction of a self-compensating pair of adiabatic pulses during an initial preparation stage reduces the sidebands below 0.06% of the intensity of the decoupled resonance. Phase evolution diagrams (*23*) have proved to be very useful for visualizing these effects.

Note added in proof. This treatment of adiabatic pulses has implicitly assumed the approximation that spin inversion occurs at the exact instant that the frequency sweep passes through the chemical shift of a given group of spins. In fact 90% spin inversion requires a frequency sweep of $4\gamma B_1/2\pi$ (hertz). However, since the total range of the adiabatic sweep is always large in comparison with the radiofrequency field intensity ($\gamma B_1/2\pi$) this is a good approximation.

REFERENCES

1. A. Abragam, ''The Principles of Nuclear Magnetism.'' Oxford Univ. Press, Oxford, 1961.
2. M. H. Levitt and R. Freeman, *J. Magn. Reson.* **33,** 473 (1979).
3. T. Fujiwara, T. Anai, N. Kurihara, and K. Nagayama, *J. Magn. Reson. A* **104,** 103 (1993).
4. Z. Starčuk, Jr., K. Bartušek, and Z. Starčuk, *J. Magn. Reson. A* **107,** 24 (1994).
5. M. R. Bendall, *J. Magn. Reson. A* **112,** 126 (1995).
6. Ē. Kupče and R. Freeman, *J. Magn. Reson. A* **115,** 273 (1995).
7. R. Fu and G. Bodenhausen, *Chem. Phys. Lett.* **245,** 415 (1995).
8. Ē. Kupče and R. Freeman, *J. Magn. Reson. A* **117,** 246 (1995).
9. R. Fu and G. Bodenhausen, *J. Magn. Reson. A* **117,** 324 (1995).
10. Ē. Kupče and R. Freeman, *J. Magn. Reson. A* **118,** 299 (1996).
11. R. Fu and G. Bodenhausen, *J. Magn. Reson. A* **119,** 129 (1996).
12. Ē. Kupče and R. Freeman, *Chem. Phys. Lett.* **250,** 523 (1996).
13. M. R. Bendall and T. E. Skinner, *J. Magn. Reson. A* **120,** 77 (1996).
14. A. Tannús and M. Garwood, *J. Magn. Reson. A* **120,** 133 (1996).
15. Ē. Kupče, R. Freeman, G. Wider, and K. Wüthrich, *J. Magn. Reson. A* **120,** 264 (1996).
16. S. Conolly, G. Glover, D. Nishimura, and A. Macovski, *Magn. Reson. Med.* **18,** 28 (1991).
17. V. L. Ermakov, J. M. Böhlen, and G. Bodenhausen, *J. Magn. Reson. A* **103,** 226 (1993).
18. T. L. Hwang and A. J. Shaka, *J. Magn. Reson. A* **112,** 275 (1995).
19. T. L. Hwang, P. C. L. van Zijl, and M. Garwood, *J. Magn. Reson.* **124,** 150 (1997).
20. R. Freeman, T. H. Mareci, and G. A. Morris, *J. Magn. Reson.* **42,** 431 (1981).
21. M. R. Bendall, D. T. Pegg, D. M. Doddrell, and J. Field, *J. Am. Chem. Soc.* **103,** 934 (1981).
22. G. A. Morris and R. Freeman, *J. Am. Chem. Soc.* **101,** 760 (1979).
23. R. Freeman, S. P. Kempsell, and M. H. Levitt, *J. Magn. Reson.* **35,** 447 (1979).
24. R. Boelens, M. Burgering, R. H. Fogh, and R. Kaptein, *J. Biomol. NMR* **4,** 201 (1994).
25. S. M. Pascal, D. R. Muhandiram, T. Yamazaki, J. D. Forman-Kay, and L. E. Kay, *J. Magn. Reson. B* **103,** 197 (1994).
26. K. Hallenga and G. M. Lippens, *J. Biomol. NMR* **5,** 59 (1995).
27. K. Ogura, H. Terasawa, and F. Inagaki, *J. Biomol. NMR* **8,** 492 (1996).
28. A. J. Shaka, P. B. Barker, C. J. Bauer, and R. Freeman, *J. Magn. Reson.* **67,** 396 (1986).
29. Ē. Kupče, R. Freeman, G. Wider, and K. Wüthrich, *J. Magn. Reson. A* **122,** 81 (1996).
30. C. P. Slichter, ''Principles of Magnetic Resonance,'' 3rd ed., Springer-Verlag, Berlin, 1996.